Impacts of tropical cyclone-heatwave compound events on surface ozone in eastern China: Comparison between the Yangtze River and Pearl River Deltas

Cuini Qi [1], Pinya Wang [1, *], Yang Yang [1, *], Huimin Li [1], Hui Zhang [1], Lili Ren [2], Xipeng Jin [1], Chenchao Zhan [3], Jianping Tang [4], Hong Liao [1]

[1]Jiangsu Key Laboratory of Atmospheric Environment Monitoring and Pollution Control, Jiangsu Collaborative Innovation Center of Atmospheric Environment and Equipment Technology, Joint International Research Laboratory of Climate and Environment Change, School of Environmental Science and Engineering, Nanjing University of Information Science and Technology, Nanjing, Jiangsu, China

[2]College of Environment and Ecology, Jiangsu Open University, Nanjing, Jiangsu, China

[3]School of Atmospheric Physics, Nanjing University of Information Science and Technology, Nanjing, Jiangsu, China

[4]School of Atmospheric Sciences, Nanjing University, Nanjing, Jiangsu, China

Correspondence to: Pinya Wang, pinya.wang@nuist.edu.cn

Yang Yang, yang.yang@nuist.edu.cn

Abstract

China has implemented some air pollution management measures in recent years, yet severe ozone pollution remains a significant issue. The Southeastern Coast of China (SECC) is often influenced by hot extremes and tropical cyclones (TCs), and the two can occur simultaneously (TC-HDs). The compound TC-HDs show a rising trend in the summers of 2014-2019, potentially affecting ozone pollution. Here, we found that surface ozone concentrations over SECC are more elevated during extreme hot days than the summer climatology. However, compared to extreme hot days alone (AHDs), the maximum 8-hour average ozone (MDA8 O_3) concentration increases by an average of 6.8 μg/m^3 in the Pearl River Delta (PRD) and decreases by 13.2 μg/m^3 in the Yangtze River Delta (YRD) during the compound TC-HDs. The meteorological conditions during AHDs favor the chemical production of ozone over SECC, exhibiting increased temperature and solar radiation and decreased relative humidity. Relative to AHDs, strong northeasterly winds prevail in SECC during TC-HDs, suggesting the potential of ozone cross-regional transport between YRD and PRD. The process analysis in the chemical transport model (GEOS-Chem) suggests that relative to AHDs, the chemical production of ozone is enhanced in YRD during TC-HDs while horizontal transport alleviates ozone pollution in YRD but worsens it in PRD through cross-regional transport. The results highlight the significant effects of cross-regional transport in modulating ozone pollution in the two megacity clusters during hot extremes accompanied by TC activities, giving insight into future ozone control measures over SECC under global warming.

1. Introduction

Tropospheric ozone (O_3) is the predominant air pollutant in addition to fine particulate matter ($PM_{2.5}$) in China (Fu et al., 2019), and it poses significant risks to human health and the ecosystem (Feng et al., 2015; Wang et al., 2017). Long-term exposure to high concentrations of ozone could lead to lung tissue damage and chronic obstructive pulmonary disease, thereby increasing premature death (Turner et al., 2016; Liu et al., 2018). Chen et al. (2023) demonstrated that the deterioration of ozone air quality is considered to be the primary factor responsible for the 90% increase in premature respiratory mortalities in China from 2013 to 2019. Furthermore, ozone can negatively impact crop yield by inhibiting plant photosynthesis, accelerating crop senescence, and reducing both yield and quality (Ainsworth et al., 2012; Song and Hao, 2023), ultimately affecting ecosystem stability (Gu et al., 2023).

To deal with the severe air pollution issues, China has implemented several pollution prevention and control measures, which are prioritized to tackle the problem of particulate matter, including the "Air Pollution Prevention and Control Action Plan" and the "Three-Year Action Plan for Winning the Blue Sky Defense Battle" (P. Wang et al., 2022). These efforts are making significant progress in lowering $PM_{2.5}$ concentrations. Z. Wang et al. (2022) indicated that the annual concentration of $PM_{2.5}$ in China has decreased by 13.41 $\mu g/m^3$ from 2014 to 2020. However, it is worth noting that most cities in China still frequently experienced severe ozone episodes (Li et al., 2019). It is demonstrated that surface ozone concentrations in most regions of China have increased by approximately 20% during the period from 2013 to 2017 (Huang et al., 2018). Also, Wei et al. (2022) recently found that both surface ozone concentration and ozone pollution days (the maximum

8-hour average ozone (MDA8 O_3) concentrations exceed 160 μg/m^3) in China exhibited an increasing trend from 2013 to 2020. Therefore, ozone pollution in China has received widespread attention over the past few decades (Ashmore, 2005; Gong and Liao, 2019; N. Wang et al., 2022).

Changes in tropospheric ozone are closely related to their precursor gases, including nitrogen oxides (NO_x) and volatile organic compounds (VOCs) (Fu and Liao, 2014; Jacob et al., 1999; Li et al., 2019). Zhang et al. (2023) revealed that an increase in biogenic volatile organic compounds (BVOCs) increased local ozone production by 23% per year in Hong Kong. Li et al. (2019) pointed out that anthropogenic NO_x emissions in China decreased by 21% from 2013 to 2017, whereas VOCs emissions changed little. Decreasing NO_x would increase ozone under the VOC-limited conditions prevailed in urban China but decrease ozone under rural NO_x-limited conditions. In addition to precursor emissions, meteorological conditions can significantly modulate surface ozone levels (Yin et al., 2019; Zhou et al., 2022). For example, severe ozone pollution commonly occurs during summertime with high temperatures, low relative humidity (RH), and strong solar radiation (Dai et al., 2023; Yin et al., 2019). Under low RH conditions, trees close the stomata (pores for exchanging CO_2 and water vapor), inhibiting the dry deposition of ozone and leading to ozone accumulation (Kavassalis and Murphy, 2017). Besides, low humidity conditions inhibit ozone breakdown as the O(^{1}D) combines with water molecules (H_2O) to produce hydroxyl radicals that promote ozone decomposition in high-humidity environments (M. Li et al., 2021). Wind direction and wind speed play an important role in the transport and diffusion of ozone (Banta et al., 2011; Jammalamadaka and Lund, 2006). It is proved that the co-occurred heat waves and atmospheric stagnation days with low wind speeds favor ozone pollution in the U.S. through promoting the ozone

82 production (Zhang et al., 2018). Reduced clouds and strengthened solar radiation during the hot
83 extremes favor photochemical ozone production in the troposphere and thus increase the surface
84 ozone concentrations (P. Wang et al., 2022). Large-scale atmospheric circulation can modulate
85 surface ozone through changing the meteorological conditions (Yang et al., 2022). For instance, the
86 stronger western Pacific subtropical high (WPSH) leads to higher temperatures, stronger solar
87 radiation, lower RH, and less precipitation, which favors the production and accumulation of surface
88 ozone in northern China (Jiang et al., 2021).

89 Extreme weather events, especially heat waves and tropical cyclones (TCs), have a significant
90 impact on ozone pollution in eastern China (Lin et al., 2019; T. Wang et al., 2017). High ozone
91 concentration events are typically associated with high temperatures, which lead to increased
92 emissions of BVOCs and enhance the chemical formation of ozone (Lu et al., 2019; P. Wang et al.,
93 2022). P. Wang et al. (2022) indicate that ozone pollution levels are significantly higher during
94 extreme heat events compared to other days in the North China Plain.TC activities can substantially
95 affect tropospheric ozone by affecting the chemical production, transport, and accumulation
96 processes over the coastal regions of China (K. Meng et al., 2022; Qu et al., 2021; Zhan et al., 2022).
97 Shu et al (2016) investigated the impacts of Typhoon Utor on an ozone pollution episode over the
98 Yangtze River Delta (YRD) of China from August 7 to 12, 2013. They found that the peripheral
99 circulations of the approaching typhoon intensified downward airflow, leading to a short-term local
100 weather pattern of high temperatures, low humidity, intense solar radiation, and light winds, which
101 exacerbated ozone pollution. Following the passage of TCs, the lower tropospheric transport of
102 ozone-rich air and strong photochemical reactions also contribute to amplifying ozone pollution

(Zhan et al., 2020). For ozone pollution in Pearl River Delta (PRD), influenced by the strong downdrafts related to the periphery of TCs, the PRD region typically is dominated by high pressure, low humidity, and strong solar radiation, leading to the accumulation of ozone (Wei et al., 2016; Ouyang et al., 2022). Moreover, TC activities are proven to enhance the chemical interactions between anthropogenic and biogenic emissions, resulting in extreme ozone pollution over both the YRD and PRD regions (N. Wang et al., 2022).

The southeastern coastal region of China (SECC), including the YRD and PRD regions, experiences both frequent TCs and heatwave events under global warming (W. Wang et al., 2016; Xiao et al., 2011). And there is a significant concurrent relationship between extreme heatwaves and TC activity that the peripheral circulations of TCs can promote extreme heatwaves (P. Wang et al., 2023; Zhang et al., 2024). Such compound hazards are more destructive than the individual extremes (Matthews et al., 2019). The SECC region has experienced a considerable rise in surface ozone concentrations during the period from 2013 to 2019 (X. Meng et al., 2022). Although the individual effects of heatwaves and TCs on ozone have been emphasized, the effects of the compound extremes of heat waves and TCs on ozone pollution have received limited attention.

In this study, we aim to investigate the impacts of the compound hazards of TCs and extreme hot days (TC-HDs) on ozone pollution in SECC (105-125° E,10-35° N) based on the long-term (2014-2019) observational records of air temperatures and TCs, reanalysis datasets of ground-level ozone concentrations and meteorological parameters, and the GEOS-Chem model simulations. The mechanisms contributing to these impacts are also analyzed. The study is organized as follows: Section 2 presents the methods and data utilized, and Section 3 describes the spatial and temporal

variations of TC-HDs observed in SECC during 2014-2019. Section 4 describes the impacts of TC-HDs on ozone concentration in SECC, with a focus on YRD and PRD regions. In Section 5, we investigate the possible mechanisms for the anomalous ozone concentrations in SECC during TC-HDs as well as the differences between YRD and PRD by investigating the meteorological conditions and key chemical and physical process analysis with the GEOS-Chem model. Finally, Section 6 provides a summary and discussion.

2. Data and methods

2.1 Observational datasets

In this work, we focus on the ozone pollution over SECC where is vulnerable to both severe hot extremes and ozone pollution (Ma et al., 2019; P. Wang et al., 2022). A topographic map of the SECC including the YRD and PRD regions is shown in Figure 1. The daily maximum air temperatures (Tmax) from observational sites in the domain for the period 2014-2019 are provided by the China Meteorological Administration (CMA). The best track dataset of TCs is also released by CMA (accessible at https:// tcdata.typhoon.org.cn/zjljsjj_sm.html). This dataset includes the time, location, and intensity of TCs, which records all TCs that have passed through the western North Pacific (WNP) since 1949 (Lu et al., 2021; Ying et al., 2014).

2.2 Reanalysis datasets

The ground-level ozone concentrations for the period 2014-2019 are obtained from the high-resolution and high-quality ground-level MDA8 ozone data (unit: $\mu g/m^3$) for China (ChinaHighO_3) at a resolution of 0.1° × 0.1°, which is one of the series of the high-resolution and high-quality ground-level air pollutants in China (Wei et al., 2022). The ChinaHighO_3 dataset provides reliable

estimates of MDA8 ozone, demonstrated by an average out-of-sample (out-of-station) coefficient of determination of 0.87 (0.80) and a root-mean-square error of 17.10 (21.10) μg/m^3 across China (Wei et al., 2022).

Meteorological parameters including 2-meter air temperature (T2m), relative humidity (RH), surface solar radiation downwards (SSRD), geopotential height (HGT), eastward wind (uwnd), northward wind (vwnd), mean sea level pressure (MSLP), total cloud cover (TCC), vertical integral of eastward water vapour flux, vertical integral of northward water vapour flux and vertically integrated moisture divergence are from the fifth generation of the European Centre for Medium-Range Weather Forecasts (ECMWF) reanalysis data (ERA5), the latest global atmospheric reanalysis of ECMWF (Hersbach et al., 2020). The temporal resolution for T2m, SSRD, and TCC is 6 hours, while that for other meteorological parameters is 3 hours, which are all utilized to generate daily mean values.

2.3 Identifications of extreme events

Severe ozone pollution episodes generally occur in SECC during summertime, coinciding with frequent heatwaves and TCs (Ji et al., et al., 2024; Shu et al., 2016). In this work, we focus on the impacts of extreme high temperatures and TCs on surface ozone during summer only (June, July, and August) in SECC, as outlined in Figure 1. P. Wang et al. (2022) pointed out that most TC tracks over the western North Pacific passed through the SECC region during their lifetimes in the past several decades. The hot days (HDs) are defined as dates when the number of high-temperature sites (Tmax≥35℃) exceeds more than 40% of the total number of observation stations within the SECC. We use the proportion of high-temperature sites exceeding 40% as a measure of HDs to ensure

adequate samples and extremely hot conditions over SECC during HDs. Note that the anomalies of surface ozone concentrations exhibit consistent spatial patterns during HDs identified by with a lower (30%) or higher (50%) criterion for the percentage of high-temperature sites (figures not shown). In this work, we classify all HDs into two categories: tropical cyclone-hot days (TC-HDs) and alone hot days (AHDs). TC-HDs are identified when hot days occur over the land regions within SECC, concurrent with the passages of tropical cyclones through the area; and AHDs indicate hot days that occur independently.

In this work, the least squares method is applied to fit the linear trend and the Student' s t-test is used to test the significance of the trend ($\alpha = 0.05$). A p-value < 0.05 indicates the statistically significant trend (as shown in Figure 2). The Student's t-test is also used to evaluate the significance of the differences in ozone concentrations and meteorological variables between HD/TC-HDs and the long-term climatology.

2.4 GEOS-Chem model

In this study, surface ozone concentrations during 2014-2019 are simulated by using the 3-D global chemical transport model (GEOS-Chem, version 13.4.1) with a horizontal resolution of 2° latitude × 2.5° longitude and 47 vertical layers from the surface to 0.01 hPa. The GEOS-Chem has the fully coupled O_3–NO_x–hydrocarbon–aerosol chemical mechanisms (Pye et al., 2009; Sherwen et al., 2016) used to simulate concentrations of gas-phase pollutants (such as ozone) and aerosols. It is driven by assimilated meteorological data of version 2 of Modern-Era Retrospective analysis for Research and Applications (MERRA2; Gelaro et al., 2017)

The anthropogenic emissions of ozone precursor gases, including CO, NOx, and non-methane

187 volatile organic compounds (NMVOCs) are provided by the Community Emissions Data System
188 (CEDS) (Hoesly et al., 2018). Methane (CH_4) concentrations are provided by the Global Monitoring
189 Division (GMD) of the National Oceanic and Atmospheric Administration (NOAA). Biomass
190 burning emissions are obtained from the Global Fire Emissions Database version 4 (GFEDv4) (Van
191 Der Werf et al., 2017). The biogenic emissions are estimated with the Model of Emissions of Gases
192 and Aerosols from Nature (MEGAN) version 2.1(Guenther et al., 2012). Our previous studies show
193 that GEOS-Chem model excels in accurately reproducing observed ozone concentrations and spatial
194 distributions in China (Yang et al., 2022, 2014).

195 Meteorological conditions can modulate surface ozone concentrations through affecting the
196 physical and chemical processes including chemical production, horizontal advection, vertical
197 advection, dry deposition and diffusion (Gong and Liao, 2019). In this work, we quantify the
198 contributions of individual processes to ozone changes using the model outputs of GEOS-Chem
199 (Gong and Liao, 2019; Ni et al., 2024; Shu et al., 2016). In the GEOS-Chem model, the change in
200 ozone over time step are caused by chemical production, horizontal advection, vertical advection,
201 dry deposition and diffusion, which can be used for separating out and quantifying the contributions
202 of individual physical and chemical processes to the changes in the simulated ozone concentrations
203 (Gong and Liao, 2019; Ni et al., 2024; Shu et al., 2016).

204 **3. Spatial and temporal variations of compound TC-HDs**

205 There are 63 days of TC-HDs over SECC during the summers of 2014-2019, accounting for
206 around 70% of the total HDs (91 days), with 28 hot days (30%) occurring alone (AHDs) in the past
207 6 years. The monthly variations of HDs, TCs, and TC-HDs over SECC from 2014 to 2019 are

displayed in Figure 2. All the weather extremes show notable intraseasonal variations with relatively higher occurrences in July and August but lower occurrences in June each year. Besides, both the occurrences of HDs and TCs demonstrate significant upward trends at the 90% confidence level, with a rate of 0.31 days per month and 0.33 days per month, respectively. TC-HDs also show an increasing trend with a rate of increase of 0.2 days/month, consistent with the variations of HDs and TCs in the past six years. Hence, it is essential to examine the effects of rising TC-HDs on ozone pollution in the SECC region.

Figure 3 demonstrates the spatial features of TC-HDs during 2014-2019. China Meteorological Administration classifies tropical cyclones into 6 classes based on their intensity, namely Tropical Depression (TD, 10.8-17.1 m/s), Tropical Storm (TS, 17.2-24.4 m/s), Strong Tropical Storm (STS, 24.5-32.6 m/s), Typhoon (TY, 32.7-41.4 m/s), Strong Typhoon (STY, 41.5-50.9 m/s) and Super Typhoon (SSTY, ≥51.0 m/s). TCs are generally stronger before their landfalls, which can reach STY and even SSTY (Fig. 3a and 3b), consistent with previous findings (Han et al., 2022; Tuleya et al., 1984). TCs that affect the SECC primarily originate east of 135° E and move westward to the eastern coastal regions. Around 90% of TCs associated with TC-HDs make landfalls while the others weaken and dissipate over the ocean. Moreover, the air temperatures over land regions of SECC during the TC-HDs are generally high, where the average Tmax of most sites are beyond 35℃ and reach up to 38℃ (Fig. 3a). Compared with the summer climatology from 2014 to 2019, the average Tmax during TC-HDs increased approximately 4℃ over most land regions of SECC (Fig. 3b).

The temporal variations of the proportion of high-temperature sites (Tmax≥ 35℃) and the

229 temperature anomalies relative to the summertime climatology averaged for the SECC land regions
230 along with the movements of TCs are given in Figs. 3c and 3d. Specifically, in Figures 3c&3d, the
231 colored dots along the movements of TC tracks represent the proportion of high-temperature sites
232 and the average temperature anomalies relative to the summertime climatology in SECC,
233 respectively. The two variables demonstrate similar patterns of variation. As TCs approach land
234 regions, both the high-temperature sites and temperature anomalies are increasing gradually, with a
235 particularly pronounced temperature increase associated with TCs moving towards the PRD regions.
236 In contrast, there is typically a decline in both the average air temperatures and the proportion of
237 high-temperature sites following the landfalls of TCs, which could be related to the strong wind and
238 rainfall associated with the TCs (Gori et al., 2022; Zhang et al. 2024).

239 **4. Influences of TC-HDs on surface ozone concentrations in SECC**

240 Extreme high temperatures and the accompanied meteorology such as high-pressure systems
241 and strong radiation can affect local ozone pollution by enhancing chemical production and/or
242 accumulation (Gong and Liao, 2019; P. Wang et al., 2022; X. Wang et al., 2009). It is also well
243 demonstrated that extreme high temperatures and TCs can affect ozone pollution in coastal regions
244 of China (Ding et al., 2023; Huang et al., 2011; N. Wang et al., 2022). In this work, we further focus
245 on the impacts of TC-HDs on surface ozone concentrations over land regions of SECC. Figure 4
246 presents the spatial distributions of ozone concentration anomalies during TC-HDs and AHDs
247 relative to the summertime climatology from 2014-2019, as well as the differences between the two.
248 Notable increases in surface ozone concentrations are observed over most land regions of SECC
249 during the AHDs period, with anomalous MDA8 ozone reaching 40 $\mu g/m^3$ and 20 $\mu g/m^3$ over the

YRD (118-122° E, 30-33° N) and PRD (110-115.5° E, 21.5-24° N) regions, respectively (Fig. 4a), consistent with previous finding that hot extremes can worsen ozone pollution (P. Wang et al., 2022). During the compound TC-HDs, most land regions except Hainan Island and the northern part to 33° N of SECC experience a significant enhancement in surface ozone concentrations, with MDA8 ozone anomalies above 20 $\mu g/m^3$ overall (Fig. 4b). Compared to AHDs, ozone concentrations in the easternmost coastal regions of China including YRD (outlined in Fig. 4c) are suppressed while ozone concentrations over the southernmost coastal regions of China including PRD (outlined in Fig. 4c) are promoted during the compound TC-HDs. Comparing to TCs occurring alone, surface ozone concentrations over most land regions of SECC increase during TC-HDs (Fig. S1), which should be attributed to the increases in air temperatures. In this work, we investigate the enhanced surface ozone concentration of PRD and the contrasting depression over YRD during the compound TC-HDs.

The temporal variations of anomalous MDA8 ozone in YRD and PRD regions relative to the summertime climatology with TC tracks during TC-HDs are shown in Figure 5. In Figures 5a&5b, the colored dots along the TCs track represents the anomalies of regional mean MDA8 ozone concentrations for YRD and PRD at that time compared with the summertime climatology for 2014-2019. Surface ozone concentrations over YRD are abnormally higher when TCs are positioned a long distance from land regions, whereas ozone concentrations fall dramatically when TCs approach and make landfall over land regions. And it should be noted that the surface ozone concentrations are elevated by the TCs moving westward YRD while most of the other TCs cause a decline in ozone concentrations with their approach to land regions, consistent with previous work (Shu et al.,

271 2016). Zhan et al. (2020) revealed that O_3 pollution episodes in YRD mainly occurred near the 24-
272 hour warning line before a TC landed on the coastline. The region was impacted by an inland wind
273 carrying substantial precursor substances from polluted areas, while approaching TCs led to
274 increased precipitation and strong winds resulting in decreased ozone concentrations. For PRD,
275 surface ozone concentrations increase noticeably when TCs approaching land regions. Particularly,
276 TCs heading northeast to YRD favor the increases in ozone concentrations in the PRD whereas the
277 other TC tracks tend to cause a reduction in surface ozone concentrations following landfalls (Fig.
278 5b).

279 **5. Possible mechanisms underlying the impacts of TC-HDs on surface ozone**

280 **5.1 The dominant synoptic circulations**

281 The synoptic meteorological conditions during AHDs and TC-HDs are analyzed to disentangle
282 the different responses of surface ozone to hot extremes superimposed by TCs. Specifically, we
283 examine the composites of daily mean air temperature at 2m (T2m), relative humidity (RH), surface
284 solar radiation downwards (SSRD), mean sea level surface (MSLP), geopotential height at 500 hPa
285 (500hPa HGT) and 10-meter wind speeds, and total cloud cover (TCC) anomalies relative to
286 summertime climatology from 2014 to 2019 during AHDs (Fig. 6) and TC-HDs (Fig. 7), as well as
287 the differences between the two periods (Fig. 8). During the AHDs period, the land regions of SECC
288 are covered by increased T2m, decreased RH, reduced TCC, and enhanced SSRD (Figs. 6a-d),
289 which are favorable for the chemical formation of ozone therein (Yin et al., 2019), supporting the
290 elevated surface ozone during AHDs as shown in Figure 4a. In the mid-upper troposphere, a band
291 of positive HGT at 500hPa (H500) anomalies predominates over most land regions of China,

292 extending northeastward to Korea (Fig. 6e). This pattern features westerly wind anomalies in the
293 northern flank and easterly wind anomalies in the southern flank, indicating a westward extension
294 and strengthening of the western North Pacific subtropical high (WNPSH). These conditions favor
295 the occurrences of hot extremes over southern China, as discussed by Luo & Lau (2017) and P.
296 Wang et al. (2018). Besides, it's noticed that negative H500 anomalies and cyclonic circulation
297 appear over the east of 125°E which are also seen at the surface (Fig. 6f) with anomalous
298 southwesterly prevails over SECC land regions at the surface (Fig. 6f). Such a low-pressure system
299 characterizes TC track which finally recurve northeastward (Fig. S2).

300 During TC-HDs, most land regions of SECC are covered by increased T2m, decreased RH,
301 reduced TCC, and enhanced SSRD (Figs. 7a-d), favoring the enhanced chemical formation of ozone
302 therein, supporting the elevated surface ozone during TC-HDs as shown in Figure 4b. In the mid-
303 upper troposphere, positive H500 anomalies cover nearly the whole land region of China with
304 maximum dominating Korea, accompanied by anomalous anticyclonic circulation. Such changes
305 characterize the strengthening and westward extension of WPSH (Fig. 7e), favoring more hot
306 extremes. A dipole pattern of MSLP anomalies can be observed at the surface, with an abnormal
307 low-pressure center over the South China Sea and another to its east (Fig. 7f). Besides, the land
308 regions are influenced by weak winds at the surface (Fig. 7f). Particularly, for the decrease MDA8
309 ozone, we can see that during TC-HDs, Hainan island is covered by decreased T2m, increased RH,
310 reduced SSRD, and increased TCC (Figs. 7a-d), along with negative H500 and MSLP anomalies
311 (Figs. 7e&f). Such meteorological conditions in Hainan islands may suppress the chemical
312 production of ozone and the oceanic winds may clean the air (Fig. 7e). On the other hand, for the

313 north part of SECC, the circulation anomalies favor strengthened southeastern moisture flow and
314 enhance the convergence of water vapor flux there (Fig. S3), which can lead to increased relative
315 humidity (Fig.7b). The local higher temperature (Fig. 7a) and humid conditions may favor
316 convection activities (P. Wang et al., 2019b), characterized increased cloud cover (Fig. 7d) and
317 decreased surface solar radiation (Fig. 7c). These meteorological conditions can inhibit the local
318 ozone production and cause a lower ozone concentration in north part of the SECC during TC-HDs.
319 Figure 8 demonstrates the differences in meteorological variables between the periods of TC-
320 HDs and AHDs. Compared to AHDs, the YRD experiences an increase in T2m of approximately
321 1℃, while the PRD experiences a decrease in T2m of around 0.5℃ during TC-HDs. In the
322 meanwhile, RH and TCC values are increased (decreased) in PRD (YRD) while SSRD values are
323 decreased (increased) in PRD (YRD) (Figs. 8a-d). The large-scale circulations in the middle-upper
324 troposphere show positive H500 anomalies over the north and northeast parts of China including
325 YRD while southern China including PRD is dominated by negative H500 anomalies, supporting
326 the increased T2m (decreased) over YRD (PRD). Moreover, a cyclonic circulation controls southern
327 China with YRD influenced by strong southeasterly winds while PRD is influenced by inland
328 northeasterly winds (Fig. 8e). The changes in MSLP show a similar pattern to H500 anomalies with
329 positive anomalies over YRD but negative anomalies over PRD, and an anomalous low-pressure
330 system is observed over South China Sea, accompanied by strong cyclonic circulation at the surface.
331 It should be noted that the YRD is influenced by strong easterly winds from the ocean which may
332 alleviate ozone pollution as shown in Figure 4c. In contrast, PRD is influenced by strong
333 northeasterly winds from inland which is opposite to the climatological southwesterlies of the

summer monsoon circulation, which may favor the accumulation of ozone pollution therein, as shown in Fig. 4c

It should be noted that the mereological conditions in YRD favor the chemical production of ozone yet reduced ozone concentrations are observed in YRD during TC-HDs relative to AHDs. The key physiochemical processes associated with the alleviated ozone pollution over YRD but worsened ozone pollution over RPD during TC-HDs relative to AHDs are explored with GEOS-Chem model simulations in the following part.

5.2 Process analysis with GEOS-Chem model simulations

In this section, process analysis is conducted in the GEOS-Chem model to quantify the contributions of each process, including net chemical production, horizontal advection, vertical advection, and mixing (diffusion and dry deposition) to the anomalous surface ozone concentrations over PRD and YRD during TC-HDs, respectively. The observed and simulated anomalous surface MDA8 ozone during TC-HDs relative to the summer climatology mean and AHDs are given in Figure S4 and the regional averages of surface MDA8 ozone concentrations over YRD and PRD are summarized in Table 1. GEOS-Chem simulation can reasonably capture the spatial pattern of anomalous surface MDA8 ozone concentrations during TC-HDs relative to the summer climatology mean (Figs. S4a and b), and relative to AHDs (Figs. S4c and d). Particularly, compared to AHDs, the simulated surface MDA8 ozone concentrations are inhibited over YRD but enhanced over PRD during TC-HDs. As listed in Table 1, compared to AHDs, during TC-HDs, the observed (simulated) average surface MDA8 ozone concentrations in the YRD decreased by 13.21 μg/m³ (21.94 μg/m³), whereas it increased by 6.8 μg/m³ (7 μg/m³) in the PRD. This suggests that the model simulation

355 can reasonably capture the opposite changes in surface MDA8 ozone concentrations over the YRD
356 and PRD during extreme HDs superimposed by TCs.

357 Figure 9 illustrates the vertical profiles of simulated daily mean ozone concentrations for YRD
358 and PRD from surface to 500 hPa for the summer climatology, TC-HDs and AHDs during 2014-
359 2019, respectively. For YRD, surface ozone concentrations are apparently higher during AHDs than
360 those during TC-HDs and summertime climatology from surface up to the 500 hPa level (Fig. 9a).
361 This indicates that the enhancements in ozone concentrations during AHDs occur not only at the
362 surface but also to the middle of the troposphere. In addition, compared with the summertime
363 climatology, ozone concentrations in YRD during TC-HDs are slightly enhanced from surface to
364 850 hPa as well as between 600 hPa and 500 hPa while suppressed between 850hPa and 600 hPa.
365 For the PRD, ozone concentrations during TC-HDs are higher than the summertime mean and AHDs
366 from the surface up to 500 hPa (Fig. 9b). The ozone concentrations during AHDs are comparable to
367 (slightly stronger than) the summertime mean below (above) 850 hPa (Fig. 9b) based on the GEOS-
368 Chem model simulation.

369 We further analyze the main physiochemical processes affecting ozone concentration,
370 including net chemical production, vertical advection, horizontal advection and mixing (the sum of
371 dry deposition and diffusion). Figures 10 and 11 show the vertical profiles of the anomaly of each
372 process during TC-HDs and AHDs, relative to the summertime climatology over the YRD and PRD,
373 as well as the differences between TC-HDs and AHDs. During AHDs, the increase in ozone
374 concentrations in the YRD from the surface to 900 hPa is primarily contributed by chemical
375 production, while transport processes tend to decrease ozone concentration. Between 900 hPa and

700 hPa, the mixing process contributes to the increases in ozone concentrations while the transport processes and chemical productions tend to decrease ozone concentrations. Between 700 hPa and 500 hPa, horizontal transport hampers ozone increase, while chemical production and vertical transport contribute to ozone enhancement (Fig. 10a). During TC-HDs, the horizontal transport exhibits a suppressive effect on ozone concentrations in the YRD from the surface up to 500 hPa whereas the chemical production contributes to increases in ozone concentration. And two processes overtake the effects of vertical transport and mixing (Fig. 10b). In comparison with AHDs, during TC-HDs, ozone concentration increases due to chemical production exceed decreases caused by horizontal transport between the surface and 850 hPa. However, between 850 hPa and 700 hPa, the decrease in ozone concentration due to horizontal transport outweighs the increase from chemical production. Overall, compared to AHDs, the chemical production contributes to increased ozone concentrations in the YRD from the surface up to 500 hPa during TC-HDs, whereas the horizontal transport tends to lower ozone concentrations. The relatively small differences in physicochemical processes between AHDs and TC-HDs around 700 hPa in the vertical profile are due to the minor effects of these processes during both AHDs and TC-HDs (not shown). As listed in Table 2, compared to AHDs, ozone chemical production plays a predominant role in enhancing ozone pollution during TC-HDs in the YRD (1.24 Gg O_3/day), whereas horizontal transport significantly depresses ozone concentration (-1.15 Gg O_3/day). As stressed above, the strong and oceanic winds along YRD can help alleviate ozone pollution. The vertical transport and mixing processes play a less important role in affecting ozone concentrations in YRD during TC-HDs.

For PRD, the horizontal transport primarily contributes to decreased ozone concentrations in

397 the PRD between the surface and 500 hPa during AHDs. The chemical production, vertical transport
398 and mixing processes exhibit promoting effects on ozone concentrations from surface to 700 hPa
399 (Fig. 11a). During TC-HDs, horizontal transport predominantly contributes to increased ozone
400 concentrations over PRD from surface to 900 hPa and between 850 hPa and 500 hPa and the
401 chemical production increases ozone concentrations between 950 hPa and 800 hPa. In contrast, the
402 mixing process and vertical transport play a dominant role in reducing ozone concentrations
403 between the surface to 900 hPa and between 900 hPa to 500 hPa respectively (Fig. 11b). Compared
404 to AHDs, during TC-HDs, transport processes predominantly contribute to the increases in ozone
405 concentrations in the PRD from the surface up to 500 hPa. Additionally, between 900 hPa and 800
406 hPa, chemical production plays a positive role in enhancing ozone concentrations. As listed in Table
407 3, during TC-HDs compared to AHDs, the horizontal transport process in the PRD exhibits a
408 significantly stronger enhancing effect on ozone concentrations from surface to 500 hPa (1.81 Gg
409 O_3/day) compared to the other three processes. Note that the summer climatology of ozone
410 concentrations in YRD is significantly higher than that in PRD (Fig. S5) and the cross-section of
411 wind anomalies demonstrates that strong winds from YRD to PRD exist during TC-HDs (Fig. S6),
412 implying strong ozone mass transport from YRD to PRD. Thus, the cross-region transport may play
413 a significant role in worsening ozone pollution over RPD during TC-HDs relative to AHDs.

414 In summary, favorable synoptic patterns during extreme hot days promote the chemical
415 production of ozone, and thus exacerbate ozone pollution over both YRD and PRD. Compared to
416 AHDs, the anomalously meteorological conditions during TC-HDs, enhance the chemical
417 production of ozone in the YRD while the horizontal transport process mitigates ozone pollution

418 therein but worsens ozone pollution in PRD though cross-regional transport, finally resulting in an
419 increase in ozone in PRD but a decrease in YRD.

420 **6. Conclusion and discussions**

421 China has implemented a series of emission reduction strategies to alleviate air pollution, and
422 $PM_{2.5}$ concentrations have decreased significantly while ozone pollution remains a major concern.
423 Ozone pollution is sensitive to meteorological conditions, especially the extreme weathers that
424 frequently strike China under global warming. Eastern China is economically developed and
425 densely populated, with serious ozone pollution. It is also vulnerable to both extreme hot weathers
426 and TCs during the summer, which can substantially affect surface ozone concentrations (Lin et al.,
427 2019; T. Wang et al., 2017). High ozone levels are generally linked to high air temperatures, which
428 increase BVOC emissions and enhance ozone formation (e.g., Lu et al., 2019; P. Wang et al., 2022).
429 TC activities can modify surface ozone concentrations by affecting the transport and accumulation
430 processes, exacerbating pollution in the YRD and PRD (e.g., Shu et al., 2016; Zhan et al., 2020).
431 The SECC region experiences both frequent TCs and heatwave events under global warming (W.
432 Wang et al., 2016; Xiao et al., 2011) which has proven to have an intrinsic concurrent relationship
433 (Matthews et al., 2019; P. Wang et al., 2023). However, the impacts of the compound extremes of
434 hot extremes and TCs on ozone pollution over SECC have received limited attention.

435 In this work, we systematically investigate the impacts of extreme hot weathers on surface
436 ozone for the summers of 2014-2019 over SECC coupled with (TC-HDs) and without TCs (AHDs).
437 The associated synoptic conditions and physicochemical processes are assessed combined
438 reanalysis dataset with the GEOS-Chem model simulations.

Results show that the surface ozone concentrations over most land regions within SECC are elevated during both TC-HDs and AHDs relative to the climatological mean, however, there are considerable differences between the changes in ozone concentrations during TC-HDs and AHDs. Relative to AHDs, the surface ozone concentrations are noticeably decreased in the YRD region but increased in the PRD region during TC-HDs periods. The meteorological conditions suggest that though YRD is influenced by higher temperature, lower humidity, and stronger radiation during TC-HDs than AHDs, it is influenced by strong and sea breezes, which aid in ozone elimination. In contrast, the PRD is influenced by the strong northeasterly winds, opposite to the climatology, and may transport ozone pollution from polluted regions. Such a hypothesis is validated with the GEOS-Chem simulation. Compared with AHDs, among all the physicochemical processes, horizontal transport plays a crucial role in increasing (reducing) ozone levels over PRD (YRD). Compared to AHDs, the horizontal transport contributes to -1.15 Gg O_3/day and 1.8 Gg O_3/day to the net changes in tropospheric ozone mass from surface to 500 hPa in YRD and PRD during TC-HDs. The findings will provide significant implications for the control measures of ozone pollution in PRD and YRD during hot extremes, to consider the significant impacts of TC activities.

Note that throughout the lifetime of tropical cyclones, their positions exert varying influences on air temperatures and surface ozone concentrations over the land regions. Extremely high temperatures are typically observed before TCs make landfalls, driven by descending motions and intensified solar radiation (Wang et al., 2023). However, the high temperatures rapidly decline once TCs make landfalls, primarily due to the accompanying strong winds and precipitation (Gori et al., 2022; Zhang et al., 2024). Similarly, surface ozone concentrations over the YRD and PRD

460 regions tend to be elevated when TCs are at a distance from the land regions but they fall
461 dramatically when TCs make landfalls (Fig. 5), consistent with previous findings (e.g., Zhan et
462 al., 2020).

463 Extreme hot weathers are projected to be more frequent and intensified in the future under the
464 continued global warming (P. Wang et al., 2019a). Moreover, it is projected that TCs and heatwave
465 compound events are projected to significantly increase in their intensity and frequency over the
466 Northwest Pacific, causing potentially enlarged population exposures for the southeastern coast of
467 China (Wu et al. 2022). Therefore, the potential impacts of extreme hot weather and the TC-HDs
468 on surface ozone over China warrants future efforts. BVOCs are important precursors of ozone, and
469 their emissions are greatly influenced by weather conditions. As revealed by N. Wang et al. (2022),
470 the TCs over Northwest Pacific could intensify the chemical interactions between anthropogenic
471 and biogenic emissions, resulting in extreme ozone pollution over YRD and PRD regions. The
472 responses of biogenic emissions during hot extremes accompanied by TCs deserve further
473 investigation.

474

475 **Data availability**

476 The ground-level ozone concentrations are obtained from the high-resolution and high-quality
477 ground-level daily maximum 8-hour average ozone (MDA8 O_3) data for China (ChinaHighO_3,
478 https://doi.org/10.5281/zenodo.4400043). Daily maximum air temperature is provided by the
479 National Meteorological Information Center of the China Meteorological Administration (CMA,
480 http://data.cma.cn/en/). The best track dataset of tropical cyclones is also released by CMA (https://

tcdata.typhoon.org.cn/zjljsjj_sm.html). Meteorological conditions data are derived from the fifth generation of ECMWF reanalysis data (ERA5, https://cds.climate.copernicus.eu/). The GEOS-Chem model is available at http://acmg.seas.harvard.edu/geos/.

Author contributions

C. Qi performed the analyses and wrote the initial draft. P. Wang and Y. Yang conceived and supervised the study. H. Li performed the GEOS-Chem simulations. P. Wang reviewed and edited the initial draft. All the authors discussed the results and contributed to the final manuscript.

Competing interests

The authors declare that they have no competing interest.

Acknowledgements

This research was supported by the National Natural Science Foundation of China (grant 42293323, 42105166, and 41975159), the National Key Research and Development Program of China (grant 2020YFA0607803 and 2019YFA0606800), Jiangsu Science Fund for Distinguished Young Scholars (grant BK20211541, Y.Y.), and the Jiangsu Science Fund for Carbon Neutrality (grant BK20220031, H.L.).

References

Ainsworth, E.A., Yendrek, C.R., Sitch, S., Collins, W.J., Emberson, L.D.: The Effects of Tropospheric Ozone on Net Primary Productivity and Implications for Climate Change, Annu. Rev. Plant Biol., 63, 637–661, https://doi.org/10.1146/annurev-arplant-042110-103829, 2012.

Ashmore, M.R.: Assessing the future global impacts of ozone on vegetation, Plant Cell Environ., 28, 949–964, https://doi.org/10.1111/j.1365-3040.2005.01341.x, 2005.

Banta, R.M., Senff, C.J., Alvarez, R.J., Langford, A.O., Parrish, D.D., Trainer, M.K., Darby, L.S., Michael Hardesty, R., Lambeth, B., Andrew Neuman, J.: Dependence of daily peak O_3 concentrations near Houston, Texas on environmental factors: Wind speed, temperature, and boundary-layer depth, Atmos. Environ., 45, 162–173, https://doi.org/10.1016/j.atmosenv.2010.09.030, 2011.

Chen, L., Liao, H., Zhu, J., Li, K., Bai, Y., Yue, X., Yang, Y., Hu, J., Zhang, M.: Increases in ozone-related mortality in China over 2013–2030 attributed to historical ozone deterioration and future population aging, Sci. Total Environ., 858, 159972, https://doi.org/10.1016/j.scitotenv.2022.159972, 2023.

Dai, H., Huang, G., Wang, J., Zeng, H.: VAR-tree model based spatio-temporal characterization and prediction of O_3 concentration in China, Ecotoxicol. Environ. Saf., 257, 114960, https://doi.org/10.1016/j.ecoenv.2023.114960, 2023.

Ding, H., Kong, L., You, Y., Mao, J., Chen, W., Chen, D., ... & Wang, X.: Effects of tropical cyclones with different tracks on ozone pollution over the Pearl River Delta region, Atmos. Res., 286, 106680, https://doi.org/10.1016/j.atmosres.2023.106680, 2023

518 Feng, Z., Hu, E., Wang, X., Jiang, L., Liu, X.: Ground-level O_3 pollution and its impacts on food
519 crops in China: A review, Environ. Pollut., 199, 42–48,
520 https://doi.org/10.1016/j.envpol.2015.01.016, 2015.
521 Fu, Y., Liao, H.: Impacts of land use and land cover changes on biogenic emissions of volatile
522 organic compounds in China from the late 1980s to the mid-2000s: implications for
523 tropospheric ozone and secondary organic aerosol, Tellus B Chem. Phys. Meteorol., 66, 24987,
524 https://doi.org/10.3402/tellusb.v66.24987, 2014.
525 Fu, Y., Liao, H., Yang, Y.: Interannual and Decadal Changes in Tropospheric Ozone in China and
526 the Associated Chemistry-Climate Interactions: A Review, Adv. Atmospheric Sci., 36, 975–
527 993, https://doi.org/10.1007/s00376-019-8216-9, 2019.
528 Gelaro, R., McCarty, W., Suárez, M. J., Todling, R., Molod, A., Takacs, L., Randles, C. A.,
529 Darmenov, A., Bosilovich, M. G., Reichle, R., Wargan, K., Coy, L., Cullather, R., Draper, C.,
530 Akella, S., Buchard, V., Conaty, A., Da Silva, A. M., Gu, W., … Zhao, B.: The Modern-Era
531 Retrospective Analysis for Research and Applications, Version 2 (MERRA-2), J. Climate, 30,
532 5419–5454, https://doi.org/10.1175/JCLI-D-16-0758.1, 2017.
533 Gong, C., Liao, H.: A typical weather pattern for ozone pollution events in North China,
534 Atmospheric Chem. Phys., 19, 13725–13740, https://doi.org/10.5194/acp-19-13725-2019,
535 2019.
536 Gori, A., Lin, N., Xi, D., & Emanuel, K.: Tropical cyclone climatology change greatly exacerbates
537 US extreme rainfall–surge hazard, Nat. Clim. Chang., 12, 171–178,
538 https://doi.org/10.1038/s41558-021-01272-7, 2022.

539 Gu, X., Wang, T., Li, C.: Elevated ozone decreases the multifunctionality of belowground
540 ecosystems, Glob. Change Biol., 29, 890–908, https://doi.org/10.1111/gcb.16507, 2023.
541 Guenther, A.B., Jiang, X., Heald, C.L., Sakulyanontvittaya, T., Duhl, T., Emmons, L.K., Wang, X.:
542 The Model of Emissions of Gases and Aerosols from Nature version 2.1 (MEGAN2.1): an
543 extended and updated framework for modeling biogenic emissions, Geosci. Model Dev., 5,
544 1471–1492, https://doi.org/10.5194/gmd-5-1471-2012, 2012.
545 Han, W., Wang, Y., & Liu, L.: The relationship between pre-landfall intensity change and post-
546 landfall weakening of tropical cyclones over China, Front. Earth Sci., 10, 1082181,
547 https://doi.org/10.3389/feart.2022.1082181, 2022.
548 H. Hersbach, B. Bell, P. Berrisford, S. Hirahara, A. Horányi, J. Muñoz-Sabater, J. Nicolas, C. Peubey,
549 R. Radu, D. Schepers, A. Simmons, C. Soci, S. Abdalla, X. Abellan, G. Balsamo, P. Bechtold,
550 G. Biavati, J. Bidlot, M. Bonavita, G. de Chiara, P. Dahlgren, D. Dee, M. Diamantakis, R.
551 Dragani, J. Flemming, R. Forbes, M. Fuentes, A. Geer, L. Haimberger, S. Healy, R. J. Hogan,
552 E. Hólm, M. Janisková, S. Keeley, P. Laloyaux, P. Lopez, C. Lupu, G. Radnoti, P. de Rosnay,
553 I. Rozum, F. Vamborg, S. Villaume, J. N. Thépaut,.: The ERA5 global reanalysis, Q. J. R.
554 Meteorol. Soc., 146(730), 1999-2049, https://doi.org/10.1002/qj.3803, 2020.
555 Hoesly, R.M., Smith, S.J., Feng, L., Klimont, Z., Janssens-Maenhout, G., Pitkanen, T., Seibert, J.J.,
556 Vu, L., Andres, R.J., Bolt, R.M., Bond, T.C., Dawidowski, L., Kholod, N., Kurokawa, J., Li,
557 M., Liu, L., Lu, Z., Moura, M.C.P., O'Rourke, P.R., Zhang, Q.: Historical (1750–2014)
558 anthropogenic emissions of reactive gases and aerosols from the Community Emissions Data
559 System (CEDS), Geosci. Model Dev., 11, 369–408, https://doi.org/10.5194/gmd-11-369-2018,

2018.

Huang, C., Chen, C. H., Li, L., Cheng, Z., Wang, H. L., Huang, H. Y., Streets, D. G., Wang, Y. J., Zhang, G. F., and Chen, Y. R.: Emission inventory of anthropogenic air pollutants and VOC species in the Yangtze River Delta region, China, Atmos. Chem. Phys., 11, 4105–4120, https://doi.org/10.5194/acp-11-4105-2011, 2011.

Huang, J., Pan, X., Guo, X., Li, G.: Health impact of China's Air Pollution Prevention and Control Action Plan: an analysis of national air quality monitoring and mortality data, Lancet Planet. Health, 2, e313–e323, https://doi.org/10.1016/S2542-5196(18)30141-4, 2018.

Jacob, D.J., Logan, J.A., Murti, P.P.: Effect of rising Asian emissions on surface ozone in the United States, Geophys. Res. Lett., 26, 2175–2178, https://doi.org/10.1029/1999GL900450, 1999.

Jammalamadaka, S.R., Lund, U.J.: The effect of wind direction on ozone levels: a case study, Environ. Ecol. Stat., 13, 287–298, https://doi.org/10.1007/s10651-004-0012-7, 2006.

Ji, X., Chen, G., Chen, J., Xu, L., Lin, Z., Zhang, K., Fan, X., Li, M., Zhang, F., Wang, H., Huang, Z., & Hong, Y.: Meteorological impacts on the unexpected ozone pollution in coastal cities of China during the unprecedented hot summer of 2022, Sci. Total Environ., 914, 170035, https://doi.org/10.1016/j.scitotenv.2024.170035, 2024.

Jiang, Z., Li, J., Lu, X., Gong, C., Zhang, L., Liao, H.: Impact of western Pacific subtropical high on ozone pollution over eastern China, Atmospheric Chem. Phys., 21, 2601–2613, https://doi.org/10.5194/acp-21-2601-2021, 2021.

Kavassalis, S.C., Murphy, J.G.: Understanding ozone-meteorology correlations: A role for dry deposition, Geophys. Res. Lett., 44, 2922–2931, https://doi.org/10.1002/2016GL071791, 2017.

Li, K., Jacob, D.J., Liao, H., Shen, L., Zhang, Q., Bates, K.H.: Anthropogenic drivers of 2013–2017 trends in summer surface ozone in China, Proc. Natl. Acad. Sci., 116, 422–427, https://doi.org/10.1073/pnas.1812168116, 2019.

Li, M., Yu, S., Chen, X., Li, Z., Zhang, Y., Wang, L., Liu, W., Li, P., Lichtfouse, E., Rosenfeld, D., and Seinfeld, J. H.: Large scale control of surface ozone by relative humidity observed during warm seasons in China, Environ. Chem. Lett., 19, 3981–3989, https://doi.org/10.1007/s10311-021-01265-0, 2021.

Lin, X., Yuan, Z., Yang, L., Luo, H., Li, W.: Impact of Extreme Meteorological Events on Ozone in the Pearl River Delta, China, Aerosol Air Qual. Res., 19, 1307–1324, https://doi.org/10.4209/aaqr.2019.01.0027, 2019.

Liu, H., Liu, S., Xue, B., Lv, Z., Meng, Z., Yang, X., Xue, T., Yu, Q., He, K.: Ground-level ozone pollution and its health impacts in China, Atmos. Environ., 173, 223–230, https://doi.org/10.1016/j.atmosenv.2017.11.014, 2018.

Lu, X., Yu, H., Ying, M., Zhao, B., Zhang, S., Lin, L., Bai, L., Wan, R.: Western North Pacific Tropical Cyclone Database Created by the China Meteorological Administration, Adv. Atmospheric Sci., 38, 690–699, https://doi.org/10.1007/s00376-020-0211-7, 2021.

Lu, X., Zhang, L., Chen, Y., Zhou, M., Zheng, B., Li, K., Liu, Y., Lin, J., Fu, T.-M., Zhang, Q.: Exploring 2016–2017 surface ozone pollution over China: source contributions and meteorological influences, Atmospheric Chem. Phys., 19, 8339–8361, https://doi.org/10.5194/acp-19-8339-2019, 2019.

Luo, M., & Lau, N.-C.: Heat Waves in Southern China: Synoptic Behavior, Long-Term Change, and

602 Urbanization Effects, J. Climate, 30(2), 703–720, https://doi.org/10.1175/JCLI-D-16-0269.1,
603 2017.
604 Ma, M., Gao, Y., Wang, Y., Zhang, S., Leung, L.R., Liu, C., Wang, S., Zhao, B., Chang, X., Su, H.,
605 Zhang, T., Sheng, L., Yao, X., Gao, H.: Substantial ozone enhancement over the North China
606 Plain from increased biogenic emissions due to heat waves and land cover in summer 2017,
607 Atmos Chem Phys., 19, 12195-12207, https://doi.org/10.5194/acp-19-12195-2019, 2019.
608 Matthews, T., Wilby, R.L., Murphy, C.: An emerging tropical cyclone–deadly heat compound hazard,
609 Nat. Clim. Change, 9, 602–606, https://doi.org/10.1038/s41558-019-0525-6, 2019.
610 Meng, K., Zhao, T., Xu, X., Hu, Y., Zhao, Yang, Zhang, L., Pang, Y., Ma, X., Bai, Y., Zhao, Yuguang,
611 Zhen, S.: Anomalous surface O_3 changes in North China Plain during the northwestward
612 movement of a landing typhoon, Sci. Total Environ., 820, 153196,
613 https://doi.org/10.1016/j.scitotenv.2022.153196, 2022.
614 Meng, X., Wang, W., Shi, S., Zhu, S., Wang, P., Chen, R., Xiao, Q., Xue, T., Geng, G., Zhang, Q.,
615 Kan, H., Zhang, H.: Evaluating the spatiotemporal ozone characteristics with high-resolution
616 predictions in mainland China, 2013–2019, Environ. Pollut., 299, 118865,
617 https://doi.org/10.1016/j.envpol.2022.118865, 2022.
618 Ni, Y., Yang, Y., Wang, H., Li, H., Li, M., Wang, P.: Contrasting changes in ozone during 2019–2021
619 between eastern China and the other regions of China, Sci. Total Environ., 908, 168272,
620 http://dx.doi.org/10.2139/ssrn.4563723, 2024.
621 Ouyang, S., Deng, T., Liu, R., Chen, J., He, G., Leung, J.C.H., Wang, N., Liu, S.C.: Impact of a
622 subtropical high and a typhoon on a severe ozone pollution episode in the Pearl River Delta,

China, Atmospheric Chem. Phys., 22(16), 10751-10767, https://doi.Org/10.5194/acp-22-10751-2022, 2022.

Pye, H.O.T., Liao, H., Wu, S., Mickley, L.J., Jacob, D.J., Henze, D.K., Seinfeld, J.H.: Effect of changes in climate and emissions on future sulfate-nitrate-ammonium aerosol levels in the United States, J. Geophys. Res. Atmospheres, 114, 2008JD010701, https://doi.org/10.1029/2008JD010701, 2009.

Qu, K., Wang, X., Yan, Y., Shen, J., Xiao, T., Dong, H., Zeng, L., Zhang, Y.: A comparative study to reveal the influence of typhoons on the transport, production and accumulation of O_3 in the Pearl River Delta, Atmospheric Chem. Phys., 21, 11593–11612, https://doi.org/10.5194/acp-21-11593-2021, 2021.

Sherwen, T., Schmidt, J.A., Evans, M.J., Carpenter, L.J., Großmann, K., Eastham, S.D., Jacob, D.J., Dix, B., Koenig, T.K., Sinreich, R., Ortega, I., Volkamer, R., Saiz-Lopez, A., Prados-Roman, C., Mahajan, A.S., Ordóñez, C.: Global impacts of tropospheric halogens (Cl, Br, I) on oxidants and composition in GEOS-Chem, Atmospheric Chem. Phys., 16, 12239–12271, https://doi.org/10.5194/acp-16-12239-2016, 2016.

Shu, L., Xie, M., Wang, T., Gao, D., Chen, P., Han, Y., Li, S., Zhuang, B., Li, M.: Integrated studies of a regional ozone pollution synthetically affected by subtropical high and typhoon system in the Yangtze River Delta region, China, Atmospheric Chem. Phys., 16, 15801–15819, https://doi.org/10.5194/acp-16-15801-2016, 2016.

Song, X., Hao, Y.: An assessment of O_3-related health risks and economic losses in typical regions of China, Front. Public Health, 11, 1194340, https://doi.org/10.3389/fpubh.2023.1194340,

2023.

Tuleya, R. E., Bender, M. A., and Kurihara, Y.: A Simulation Study of the Landfall of Tropical Cyclones, Mon. Wea. Rev., 112, 124–136, https://doi.org/10.1175/1520-0493(1984)112<0124:ASSOTL>2.0.CO;2, 1984.

Turner, M.C., Jerrett, M., Pope, C.A., Krewski, D., Gapstur, S.M., Diver, W.R., Beckerman, B.S., Marshall, J.D., Su, J., Crouse, D.L., Burnett, R.T.: Long-Term Ozone Exposure and Mortality in a Large Prospective Study, Am. J. Respir. Crit. Care Med, 193, 1134–1142, https://doi.org/10.1164/rccm.201508-1633OC, 2016.

Van Der Werf, G.R., Randerson, J.T., Giglio, L., Van Leeuwen, T.T., Chen, Y., Rogers, B.M., Mu, M., Van Marle, M.J.E., Morton, D.C., Collatz, G.J., Yokelson, R.J., Kasibhatla, P.S.: Global fire emissions estimates during 1997–2016, Earth Syst. Sci. Data, 9, 697–720, https://doi.org/10.5194/essd-9-697-2017, 2017.

Wang, N., Huang, X., Xu, J., Wang, T., Tan, Z., Ding, A.: Typhoon-boosted biogenic emission aggravates cross-regional ozone pollution in China, Sci. Adv., 8, eabl6166, https://doi.org/10.1126/sciadv.abl6166, 2022.

Wang, P., Hui, P., Xue, D., & Tang, J.: Future projection of heat waves over China under global warming within the CORDEX-EA-II project, Clim. Dynam., 53(1–2), 957–973, https://doi.org/10.1007/s00382-019-04621-7, 2019a.

Wang, P., Leung, L. R., Lu, J., Song, F., & Tang, J.: Extreme wet-bulb temperatures in China: The significant role of moisture, J. Geophys. Res.: Atmos., 124(22), 11944–11960, https://doi.org/10.1029/2019JD031477, 2019b.

Wang, P., Tang, J., Wang, S., Dong, X., & Fang, J.: Regional heatwaves in china: a cluster analysis, Clim. Dynam., 50, 1901–1917, https://doi.org/10.1007/s00382-017-3728-4, 2018.

Wang, P., Yang, Y., Li, H., Chen, L., Dang, R., Xue, D., Li, B., Tang, J., Leung, L.R., Liao, H.: North China Plain as a hot spot of ozone pollution exacerbated by extreme high temperatures, Atmospheric Chem. Phys., 22, 4705–4719, https://doi.org/10.5194/acp-22-4705-2022, 2022.

Wang, P., Yang, Y., Xue, D., Qu, Y., Tang, J., Leung, L.R., Liao, H.: Increasing Compound Hazards of Tropical Cyclones and Heatwaves over Southeastern Coast of China under Climate Warming, J. Clim., 36, 2243–2257, https://doi.org/10.1175/JCLI-D-22-0279.1, 2023.

Wang, T., Xue, L., Brimblecombe, P., Lam, Y.F., Li, L., Zhang, L.: Ozone pollution in China: A review of concentrations, meteorological influences, chemical precursors, and effects, Sci. Total Environ., 575, 1582–1596, https://doi.org/10.1016/j.scitotenv.2016.10.081, 2017.

Wang, T., Zhong, Z., Sun, Y., Wang, J.: Impacts of tropical cyclones on the meridional movement of the western Pacific subtropical high, Atmospheric Sci. Lett., 20, e893, https://doi.org/10.1002/asl.893, 2019.

Wang, W., Zhou, W., Li, X., Wang, X., Wang, D.: Synoptic-scale characteristics and atmospheric controls of summer heat waves in China, Clim. Dynam., 46, 2923–2941, https://doi.org/10.1007/s00382-015-2741-8, 2016.

Wang, X., Chen, F., Wu, Z., Zhang, M., Tewari, M., Guenther, A., & Wiedinmyer, C.: Impacts of weather conditions modified by urban expansion on surface ozone: Comparison between the Pearl River Delta and Yangtze River Delta regions, Adv. Atmos. Sci., 26, 962–972, https://doi.org/10.1007/s00376-009-8001-2, 2009.

686 Wang, Z., Hu, B., Zhang, C., Atkinson, P.M., Wang, Z., Xu, K., Chang, J., Fang, X., Jiang, Y., Shi,
687 Z.: How the Air Clean Plan and carbon mitigation measures co-benefited China in $PM_{2.5}$
688 reduction and health from 2014 to 2020, Environ. Int., 169, 107510
689 https://doi.org/10.1016/j.envint.2022.107510, 2022.
690 Wei, J., Li, Z., Li, K., Dickerson, R.R., Pinker, R.T., Wang, J., Liu, X., Sun, L., Xue, W., Cribb, M.:
691 Full-coverage mapping and spatiotemporal variations of ground-level ozone (O_3) pollution
692 from 2013 to 2020 across China, Remote Sens. Environ., 270, 112775,
693 https://doi.org/10.1016/j.rse.2021.112775, 2022.
694 Wei, X., Lam, K. S., Cao, C., Li, H., & He, J.: Dynamics of the Typhoon Haitang Related High
695 Ozone Episode over Hong Kong, Adv. Atmospheric Sci., 6089154,
696 https://doi.org/10.1155/2016/6089154, 2016.
697 Wu, J., Chen, Y., Liao, Z., Gao, X., Zhai, P., & Hu, Y.: Increasing risk from landfalling tropical
698 cyclone-heatwave compound events to coastal and inland China, Environ. Res. Lett., 17(10),
699 105007, https://doi.org/10.1088/1748-9326/ac9747, 2022.
700 Xiao, Y.F., Duan, Z.D., Xiao, Y.Q., Ou, J.P., Chang, L., Li, Q.S.: Typhoon wind hazard analysis for
701 southeast China coastal regions, Struct. Saf., 33, 286–295,
702 https://doi.org/10.1016/j.strusafe.2011.04.003, 2011.
703 Yang, Y., Li, M., Wang, H., Li, H., Wang, P., Li, K., Gao, M., Liao, H.: ENSO modulation of
704 summertime tropospheric ozone over China, Environ. Res. Lett., 17, 034020,
705 https://doi.org/10.1088/1748-9326/ac54cd, 2022.
706 Yang, Y., Liao, H., Li, J.: Impacts of the East Asian summer monsoon on interannual variations of

summertime surface-layer ozone concentrations over China, Atmospheric Chem. Phys., 14, 6867–6879, https://doi.org/10.5194/acp-14-6867-2014, 2014.

Yin, Z., Cao, B., Wang, H.: Dominant patterns of summer ozone pollution in eastern China and associated atmospheric circulations, Atmospheric Chem. Phys., 19, 13933–13943, https://doi.org/10.5194/acp-19-13933-2019, 2019.

Ying, M., Zhang, W., Yu, H., Lu, X., Feng, J., Fan, Y., Zhu, Y., Chen, D.: An Overview of the China Meteorological Administration Tropical Cyclone Database, J. Atmospheric Ocean. Technol., 31, 287–301, https://doi.org/10.1175/JTECH-D-12-00119.1, 2014.

Zhan, C., & Xie, M.: Exploring the link between ozone pollution and stratospheric intrusion under the influence of tropical cyclone Ampil, Sci. Total Environ., 828, 154261, https://doi.org/10.1016/j.scitotenv.2022.154261, 2022.

Zhan, C., Xie, M., Huang, C., Liu, J., Wang, T., Xu, M., Ma, C., Yu, J., Jiao, Y., Li, M., Li, S., Zhuang, B., Zhao, M., & Nie, D.: Ozone affected by a succession of four landfall typhoons in the Yangtze River Delta, China: Major processes and health impacts, Atmospheric Chem. Phys., 20(22), 13781–13799, https://doi.org/10.5194/acp-20-13781-2020, 2020.

Zhang, J., Gao, Y., Luo, K., Leung, L.R., Zhang, Y., Wang, K., Fan, J.: Impacts of compound extreme weather events on ozone in the present and future, Atmospheric Chem. Phys., 18, 9861–9877, https://doi.org/10.5194/acp-18-9861-2018, 2018.

Zhang, M., Yang, Y., Zhan, C., Zong, L., Gul, C., & Wang, M.: Tropical cyclone-related heatwave episodes in the Greater Bay Area, China: Synoptic patterns and urban-rural disparities. Weather and Climate Extremes, 44, 100656. https://doi.org/10.1016/j.wace.2024.100656, 2024.

Zhang, Y., Dai, J., Li, Q., Chen, T., Mu, J., Brasseur, G., Wang, T., Xue, L.: Biogenic volatile organic compounds enhance ozone production and complicate control efforts: Insights from long-term observations in Hong Kong, Atmos. Environ., 309, 119917, https://doi.org/10.1016/j.atmosenv.2023.119917, 2023.

Zhou, Y., Yang, Y., Wang, H., Wang, J., Li, M., Li, H., Wang, P., Zhu, J., Li, K., Liao, H.: Summer ozone pollution in China affected by the intensity of Asian monsoon systems, Sci. Total Environ., 849, 157785, https://doi.org/10.1016/j.scitotenv.2022.157785, 2022.

736 **Table 1.** Observed and simulated averaged surface MDA8 ozone (μg/m^3) in the Yangtze River Delta
737 (YRD, 118-122° E, 30-33° N) and the Pearl River Delta (PRD, 110-115.5° E, 21.5-24° N) during
738 TC-HDs and AHDs, as well as their differences (TC-HDs minus AHDs).

	YRD		**PRD**	
	Observed	Simulated	Observed	Simulated
TC-HDs	134.71	177.17	97.93	123.91
AHDs	147.92	199.11	91.13	116.91
Differences	−13.21	−21.94	6.8	7

739

740 **Table 2.** Contributions of difference processes for the anomalous ozone mass (Gg O_3/day) from
741 surface to 500 hPa for TC-HDs and AHDs relative to the summer climatology and their difference
742 (TC-HDs minus AHDs) for YRD.

	Net chemical production	Vertical advection	Horizontal advection	Mixing
TC-HDs	1.70	0.03	−2.18	0.004
AHDs	0.46	−0.04	−1.03	−0.12
Differences	1.24	0.07	−1.15	0.12

743

744

745

746 **Table 3.** Contributions of difference processes for the anomalous ozone mass (Gg O_3/day) from
747 surface to 500 hPa for TC-HDs and AHDs relative to the summer climatology and their difference
748 (TC-HDs minus AHDs) for PRD.

	Net chemical production	Vertical advection	Horizontal advection	Mixing
TC-HDs	0.21	−0.13	0.97	−0.002
AHDs	0.06	0.09	−0.84	−0.05
Differences	0.15	−0.22	1.81	0.05

749
750

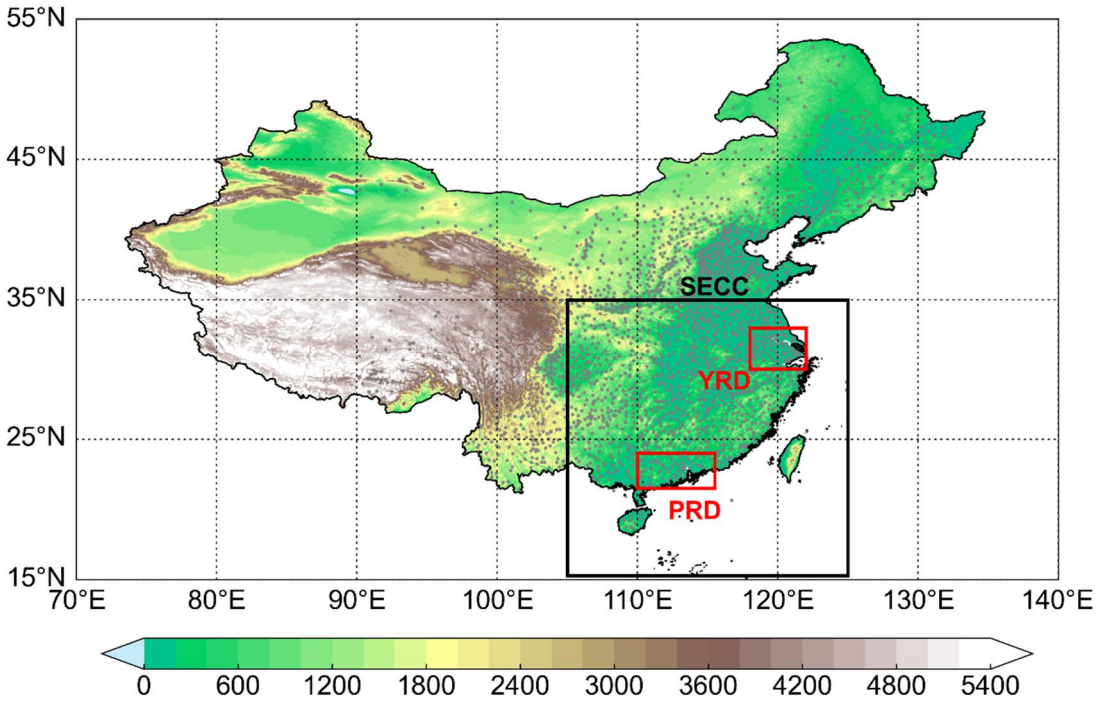

751

752 **Figure 1.** Topographic map of China with SECC (black box) and megacity clusters YRD and PRD

753 outlined (red boxes). Gray points represent the temperature observation stations.

754

755

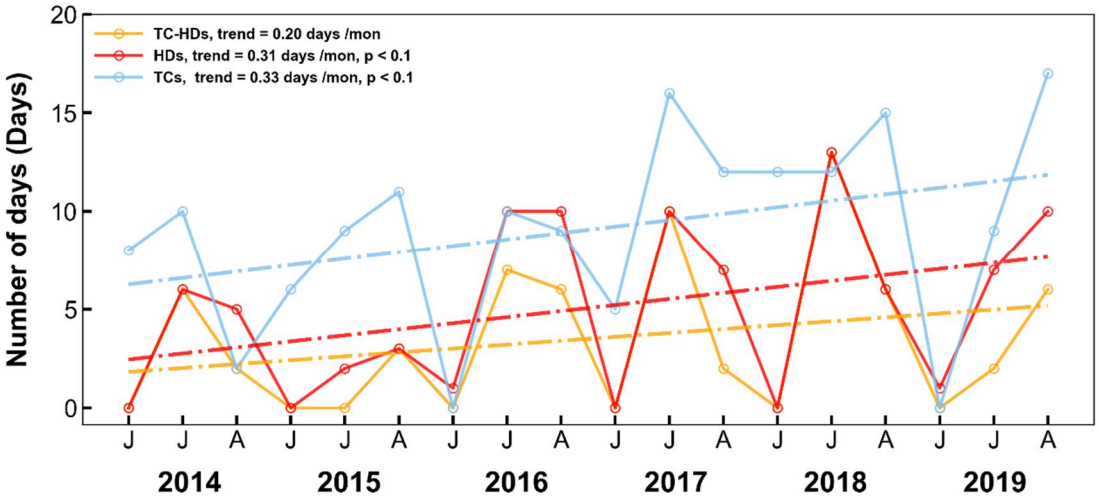

Figure 2. Monthly variations of the number of days of TC-HDs, total HDs, and total TCs during the summer season (June, July and August) from 2014-2019.

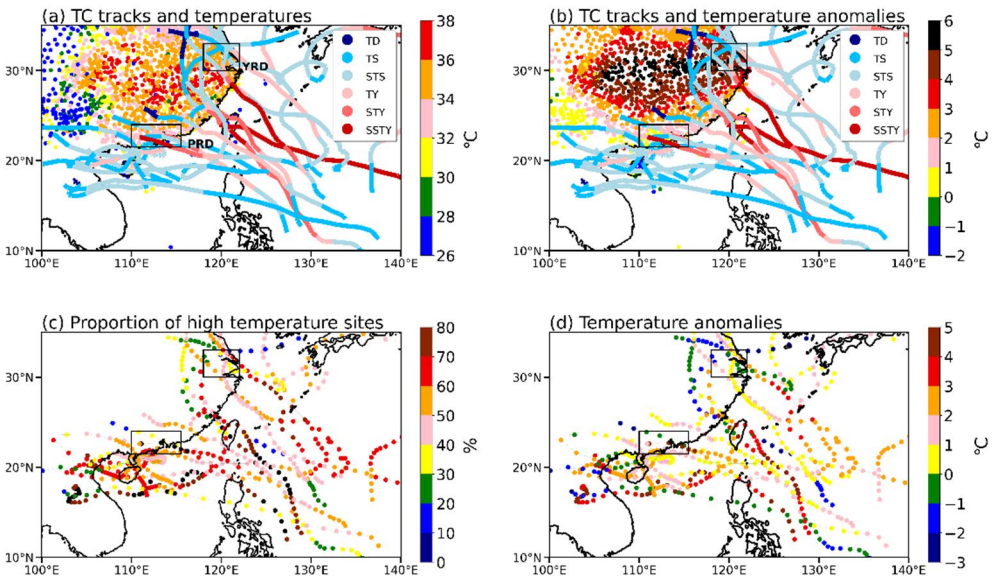

760

761 **Figure 3.** (a) The distribution of average Tmax (dots) and TC tracks during TC-HDs. (b) The Area

762 average of Tmax anomalies during TC-HDs period relative to the summer climatology (June to

763 August of 2014-2019), along with the TC tracks categorized by different intensities. (c) The

764 proportion of high-temperature sites (Tmax $\geqslant$ 35℃) over land region of SECC along with the

765 movements of the TCs. The proportion of high-temperature sites refers to the percentage of high-

766 temperature sites within all stations in the SECC region. (d) The average of Tmax anomalies for all

767 observational sites within SECC relative to the summer climatology, along with the movements of

768 TCs. YRD and PRD regions are outlined in black boxes in each panel.

769

770 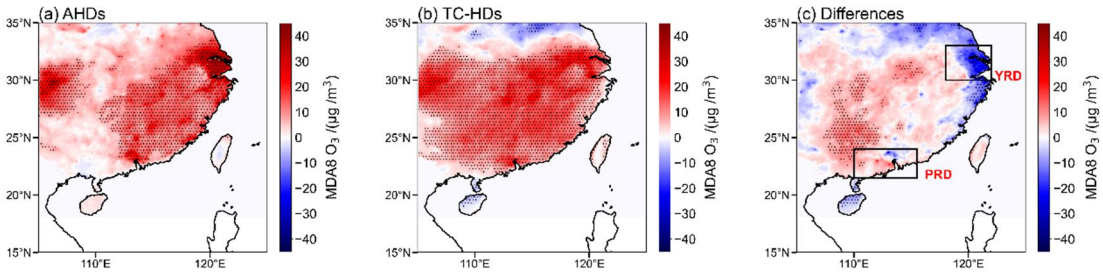

771 **Figure 4.** The spatial distribution of surface MDA8 ozone concentration anomalies during the
772 periods of (a) AHDs, (b) TC-HDs relative to the summertime climatology, as well as (c) their
773 differences (TC-HDs minus AHDs). Stippling regions indicate ozone anomalies that are
774 significantly difference from zero at the 95% confidence level. YRD and PRD regions are outlined
775 in black boxes in panel c.
776

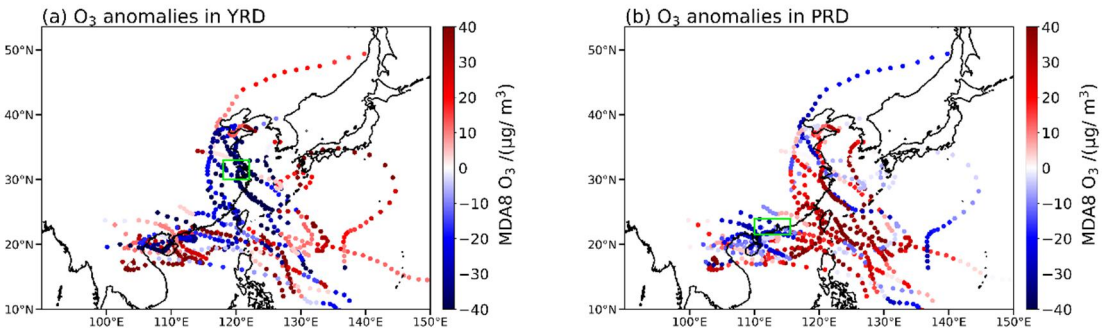

777

778 **Figure 5.** The average anomalies of surface MDA8 ozone concentrations over land regions of SECC

779 along with the movements of TCs associated with TC-HDs for (a) YRD and (b) PRD regions. YRD

780 (a) and PRD (b) regions are outlined in green boxes in panel (a) or (b).

781

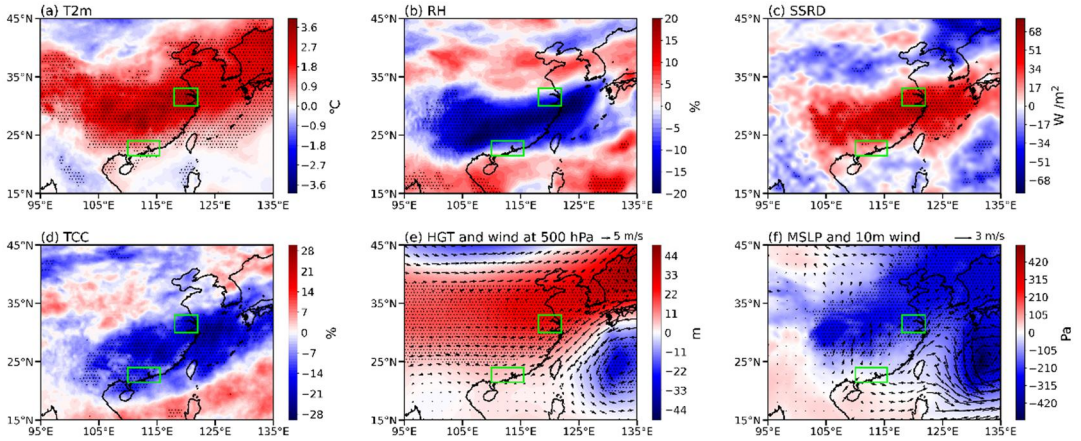

782

783 **Figure 6.** The spatial distribution for the composites anomalies of (a) air temperature at 2m (T2m),

784 (b) relative humidity (RH), (c) surface solar radiation downwards (SSRD), (d) total cloud cover

785 (TCC), (e) geopotential height (HGT) and winds at 500hPa, and (f) mean surface level pressure

786 (MSLP) and 10-meter winds during AHDs relative to the summer climatology. Stippling indicates

787 statistically significant anomalies above 95% confidence level. YRD and PRD regions are outlined

788 in green boxes in each panel.

789

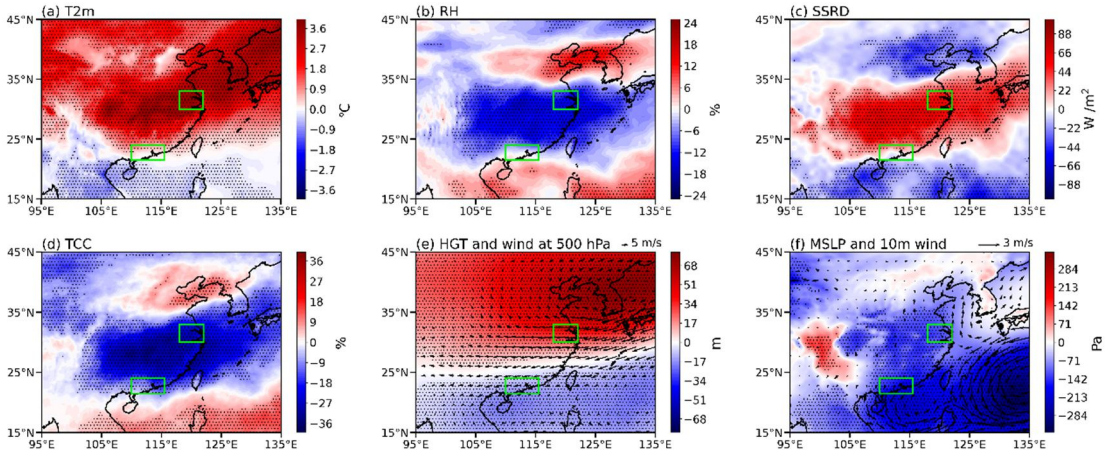

790

791 **Figure 7.** Same as in Figure 6, but for the anomalous meteorological conditions during TC-HDs.

792

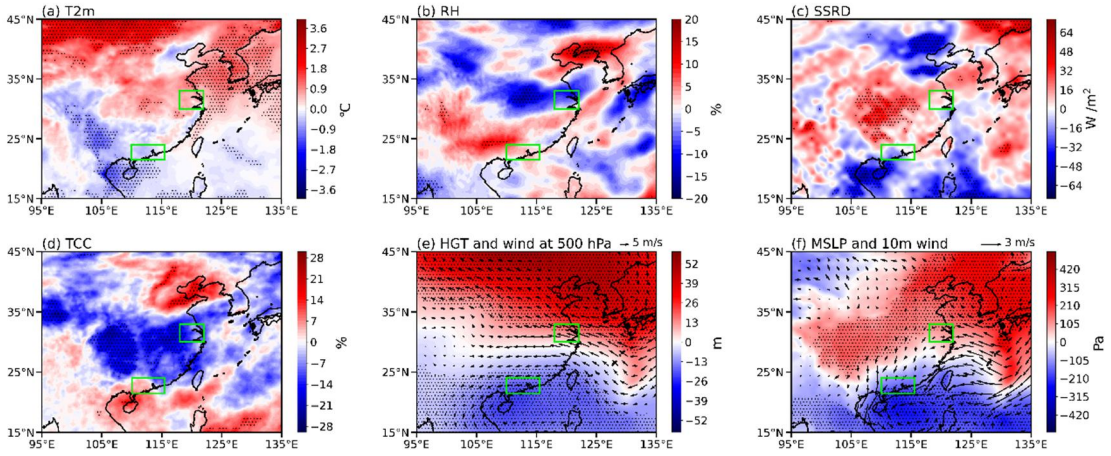

793

794 **Figure 8.** Same as in Figure 6, but for the differences between TC-HDs and AHDs (TC-HDs minus

795 AHDs).

796

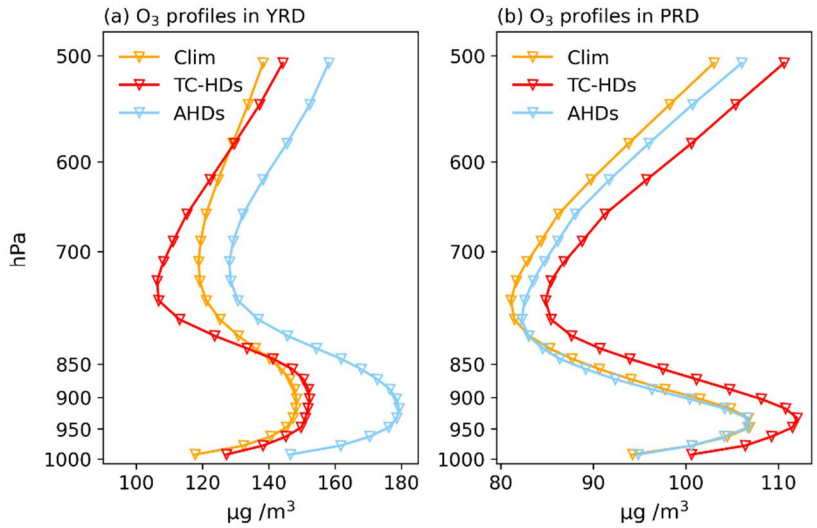

797

798 **Figure 9.** Vertical profiles of simulated daily ozone concentrations (μg/m^3) averaged over land

799 regions of SECC for TC-HDs, AHDs and for the summertime climatology (Clim) during 2014-2019

800 for (a) YRD and (b) PRD.

801

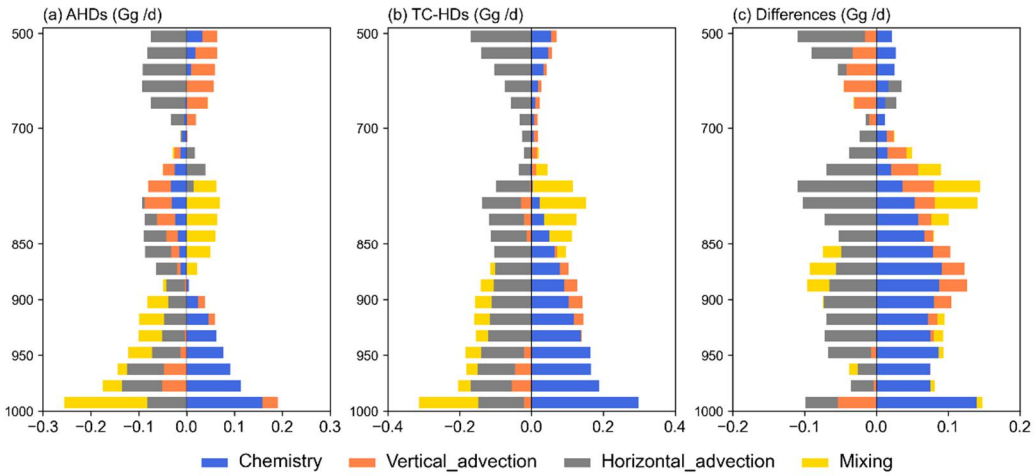

802

803 **Figure 10.** Vertical profiles of net changes in ozone mass (Gg O_3/day) anomalies averaged for YRD

804 for each process during (a) AHDs, (b) TC-HDs relative to summertime climatology, and their

805 differences (TC-HDs minus AHDs).

806

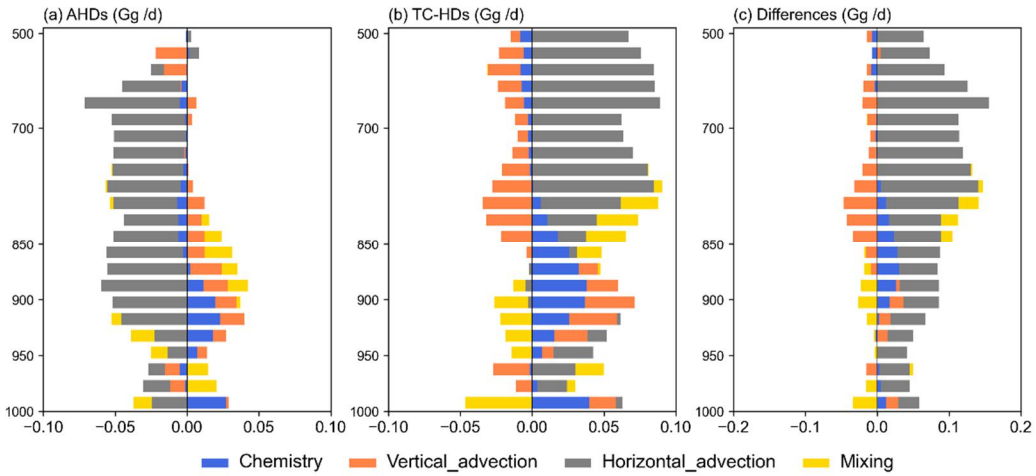

807

808 **Figure 11.** Same as in Figure 10, but for the vertical profiles of net changes in ozone mass (Gg

809 O_3/day) anomalies averaged for PRD for each process.